

Extraction of shear viscosity in stationary states of relativistic particle systems

F. Reining,¹ I. Bouras,¹ A. El,¹ C. Wesp,¹ Z. Xu,^{1,2} and C. Greiner¹

¹*Institut für Theoretische Physik, Johann Wolfgang Goethe-Universität,*

Max-von-Laue-Str. 1, D-60438 Frankfurt am Main, Germany

²*Frankfurt Institute for Advanced Studies,*

Ruth-Moufang-Str. 1, D-60438 Frankfurt am Main, Germany

(Dated: May 15, 2022)

Starting from a classical picture of shear viscosity we construct a stationary velocity gradient in a microscopic parton cascade. Employing the Navier-Stokes ansatz we extract the shear viscosity coefficient η . For elastic isotropic scatterings we find an excellent agreement with the analytic values. This confirms the applicability of this method. Furthermore for both elastic and inelastic scatterings with pQCD based cross sections we extract the shear viscosity coefficient η for a pure gluonic system and find a good agreement with already published calculations.

PACS numbers: 47.75.+f, 12.38.Mh, 25.75.-q, 66.20.-d

I. INTRODUCTION

Recent results of the Relativistic Heavy Ion Collider (RHIC) and of the Large Hadron Collider (LHC) indicate the formation of a new state of matter, the quark-gluon plasma (QGP), in relativistic heavy-ion collisions. The large value of the elliptic flow coefficient v_2 observed in these experiments [1–4] leads to the indication that the QGP behaves like a nearly perfect fluid. This has been confirmed by calculations of viscous hydrodynamics [5–11] and microscopic transport calculations [12, 13]. However, the shear viscosity coefficient η has a finite value, possibly close to the conjectured lower bound $\eta/s = 1/4\pi$ from the correspondence between conformal field theory and string theory in an Anti-de-Sitter space [14]. In comparison to ideal hydrodynamic calculations [15], dissipative hydrodynamic formalisms with finite η/s ratio [5–11] demonstrate a better agreement of the differential elliptic flow $v_2(p_t)$ with experimental data. The shear viscosity is therefore an important

parameter in viscous hydrodynamics but needs to be calculated from microscopic theory.

The η/s ratio was obtained in a full leading order perturbative QCD calculation in Ref. [16]. The Boltzmann-Vlasov equation and quasi-particle picture were recently employed to calculate the η/s ratio of a gluon gas in Ref. [17]. The shear viscosity coefficient has also been extracted from microscopic transport calculations with BAMPS (Boltzmann Approach of Multi Parton Scatterings) simulations [18, 19] using expressions based on a first-order gradient expansion of the Boltzmann Equation [20] and the entropy principle underlying the second-order Israel-Stewart hydrodynamics [21].

The goal of this work is to extract the shear viscosity coefficient η numerically from microscopic calculations using a standard setup motivated by the classical textbook picture [22, 23]. In Fig. 1 we introduce a particle system embedded between two plates. The two

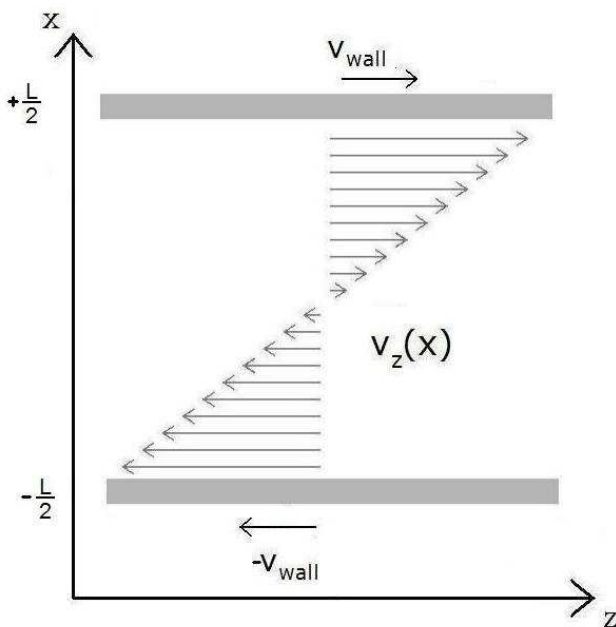


FIG. 1: The classical definition of shear viscosity. Two plates moving in opposite directions with velocity $\pm v_{\text{wall}}$. A flow gradient is established between the plates. The viscosity is proportional to the frictional force.

plates move in opposite directions each with velocity v_{wall} in z -direction. The moving walls are supplemented by two thermal reservoirs with $\pm v_{\text{wall}}$. In x -direction the system has an extension of size L . In y - and z -direction the system is homogeneous and can be of infinite size. The mean free path of the particles should be very small compared to the system size, i.e. $\lambda_{\text{mfp}} \ll L$. On a sufficiently long time-scale a stationary velocity field $v_z(x)$ should be

established. In the non-relativistic limit the velocity field is linear. With the Navier-Stokes-ansatz the shear stress tensor $\pi^{\mu\nu}$ is proportional to the gradient of the velocity

$$\pi^{xz} = -\eta \frac{\partial v_z(x)}{\partial x}. \quad (1)$$

The proportionality factor is defined to be the shear viscosity coefficient η . In Sec. II we give basic definitions and information on the numerical model we use. In Sec. III we demonstrate that Eq. (1) does not hold in general for the relativistic case, where the gradient is not necessarily linear and we discuss the shape of an ideal relativistic velocity gradient. Furthermore we will discuss the effect of viscosity and finite size effects on the velocity profile in Sec. III, where an analytical formulation for the shape of the velocity profile is derived. We employ BAMPS to reproduce the velocity gradient as discussed in this chapter. In Sec. IV we compare the numerical results for the shear viscosity coefficient η to an analytical value in order to confirm the applicability of our method. Finally we present the results on shear viscosity to entropy density ratio obtained from BAMPS with cross sections based on perturbative quantum chromodynamics (pQCD) and compare them to existing calculations. We close with a summary.

II. BASIC IDEA AND DEFINITIONS

When systems are in stationary states, the first-order Navier-Stokes formulation of relativistic viscous hydrodynamics can be used to calculate the shear viscosity η , which is the proportionality factor between the shear tensor $\pi^{\mu\nu} = T^{\langle\mu\nu\rangle}$ and the velocity gradient $\nabla^{\langle\mu}u^{\nu\rangle}$:

$$\pi^{\mu\nu} = 2\eta \nabla^{\langle\mu}u^{\nu\rangle}, \quad (2)$$

where the projection

$$B^{\langle\mu\nu\rangle} \equiv \left[\frac{1}{2} (\Delta_\alpha^\mu \Delta_\beta^\nu + \Delta_\alpha^\nu \Delta_\beta^\mu) - \frac{1}{3} \Delta^{\mu\nu} \Delta_{\alpha\beta} \right] B^{\alpha\beta} \quad (3)$$

denotes the symmetric traceless part of the tensor $B^{\mu\nu}$. $\Delta^{\mu\nu} = g^{\mu\nu} - u^\mu u^\nu$ is the transverse projection operator and the metric is $g^{\mu\nu} = \text{diag}(1, -1, -1, -1)$.

Some definitions are in order. We use the Landau's definition of the hydrodynamic four-velocity [25]:

$$u^\mu = \frac{T^{\mu\nu} u_\nu}{e}, \quad (4)$$

where

$$T^{\mu\nu} = \int \frac{d^3p}{(2\pi)^3 p^0} p^\mu p^\nu f(x, p) \quad (5)$$

is the energy-momentum tensor and the local energy density is defined as

$$e = u_\mu T^{\mu\nu} u_\nu. \quad (6)$$

The shear tensor $\pi^{\mu\nu}$ is the difference of $T^{\mu\nu}$ to its equilibrium value. For the geometry depicted in Fig. 1 $u^\mu = \gamma(1, 0, 0, v_z)$ with $\gamma = 1/\sqrt{1 - v_z^2}$.

We will build up stationary states of particle systems via numerical simulations, which are realized by employing the microscopic transport model BAMPS, which solves the Boltzmann equations for on-shell particles within a stochastic model [18, 19]. In principle any microscopic transport model can be used for this purpose.

Local values of $\pi^{\mu\nu}$ and u^μ can be easily extracted from the numerical simulations by averaging over all particles contained in a bin of size Δx . However, to obtain the gradient of u^μ one has to take values from neighbouring local cells, which would cause additional numerical errors. To avoid such numerical problem we will first derive the analytical form of $v_z(x)$ for the given setup in Fig. 1. Then we use this form and the numerically extracted $\pi^{\mu\nu}$ to calculate the shear viscosity.

III. VELOCITY, RAPIDITY AND FINITE SIZE EFFECT

A. Analytical Derivation

Instead of the hydrodynamic velocity $v_z(x)$ we address the position dependence of the rapidity $y(x)$, which is defined by

$$y(x) = \frac{1}{2} \ln \frac{1 + v_z(x)}{1 - v_z(x)}. \quad (7)$$

Thus, $v_z(x) = \tanh y(x)$. In the non-relativistic limit, where $v_z(x)$ is small, we have $v_z(x) \approx y(x)$. The advantage of $y(x)$ is that it gets a shift by a Lorentz-boost e.g. with $v_z(x_A)$

$$\Lambda_{v_z(x_A)}[y(x)] = y(x) - y(x_A). \quad (8)$$

Demanding boost-invariance, i.e., $\Lambda_{v_z(x_A)}[y(x)] = y(x - x_A)$, we obtain the solution $y(x) = ax + b$, where a and b are constant. Due to the boundary condition $y(x = \pm L/2) = \pm y_{wall}$,

$y(x)$ is symmetric in x and thus, $b = 0$. If $y(x)$ is continuous at the boundaries, we have

$$y(x) = \frac{2y_{wall}}{L} x. \quad (9)$$

In the following we will convince ourselves from relativistic kinetic theory that Eq. (9) is only valid if the particle mean free path vanishes, or the distance L between two plates is infinitely long. For a non-vanishing mean free path and a finite distance L we will see discontinuities of $y(x)$ at the boundaries. This is referred to as a finite size effect.

We consider a general local observable $A(x, t)$ with the definition

$$A(x, t) = \frac{1}{n(x, t)} \int d\Gamma_1 F_A(p_1) f(p_1; x, t), \quad (10)$$

where $d\Gamma_1 = d^3p_1/(2\pi)^3$ and $n(x, t) = \int d\Gamma_1 f(p_1; x, t)$ is the particle number density. p denotes the particle four-momentum. In our case n does not depend on position and time. In particular, for $F_A(p_1) = np_1^\mu/p_1^0$ we have the definition of particle four-flow $A(x, t) = N^\mu(x, t)$; for $F_A(p_1) = \frac{1}{2} \ln[(p_1^0 + p_1^z)/(p_1^0 - p_1^z)]$ we obtain the rapidity $A(x, t) = y(x, t)$ as given in Eq. (7), when using the Landau definition of the hydrodynamic four-velocity. For stationary states $A(x, t)$ and the particle distribution function $f(p; x, t)$ are constant in time.

We define $\tilde{f}(p; x, t) = f(p; x, t)/n(x, t)$, which is the probability density for the occurrence of a particle with momentum p around $d\Gamma$ at (x, t) . One obtains $\tilde{f}(p; x, t)$ by summing probabilities for such events that a collision at (x', t') makes a particle having the momentum p and this particle travels to x at t without further collisions. It is mathematically expressed by

$$\begin{aligned} \tilde{f}(p_1; x, t) = & \theta(p_{1x}) \int_{-\infty}^x dx' w_{gain}(p_1; x', t') w_{free}(p_1; x', t'; x, t) + \\ & \theta(-p_{1x}) \int_x^{\infty} dx' w_{gain}(p_1; x', t') w_{free}(p_1; x', t'; x, t), \end{aligned} \quad (11)$$

where $w_{gain}(p_1; x', t')$ denotes the probability density that a particle with momentum p_1 is created via a collision at (x', t') , and $w_{free}(p_1; x', t'; x, t)$ the probability that this particle travels from (x', t') to (x, t) without further collisions. Because $\tilde{f}(p; x, t)$ is invariant under the transformation $p \rightarrow -p$, the two integrals in Eq. (11) are equal. Thus,

$$\tilde{f}(p_1; x, t) = \frac{1}{2} \int_{-\infty}^{\infty} dx' w_{gain}(p_1; x', t') w_{free}(p_1; x', t'; x, t). \quad (12)$$

Our goal is to find the relation between $A(x, t)$ and $A(x', t')$, which then can be used to solve $A(x, t)$ analytically when the boundary conditions are given.

Using the standard definition of cross section for binary collisions of identical particles

$$\sigma_{22} = \frac{1}{4s} \int \frac{d\Gamma_1}{2p_1^0} \frac{d\Gamma_2}{2p_2^0} |M_{1'2' \rightarrow 12}|^2 (2\pi)^4 \delta^{(4)}(p'_1 + p'_2 - p_1 - p_2), \quad (13)$$

where $M_{1'2' \rightarrow 12}$ is the matrix element and $s = (p_1 + p_2)^2 = (p'_1 + p'_2)^2$ is the invariant mass, we have

$$w_{gain}(p_1; x', t') dx' = \frac{1}{n} \int d\Gamma'_1 d\Gamma'_2 f(p'_1; x', t') f(p'_2; x', t') v_{rel} \frac{d\sigma_{22}}{d\Gamma_1} dt'. \quad (14)$$

$v_{rel} = s/(2p_1^0 p_2^0)$ denotes the relative velocity for massless particles. dt' is the average time interval, during which a particle travels through dx' : $dt' = dx' < |p'_x|/p'_0 >^{-1}$ and $< |p'_x|/p'_0 > = 1/2$ in thermal equilibrium.

The probability $w_{free}(p_1; x', t'; x, t)$ is a product of $w_{free}(p_1; x'', t''; x'' + dx'', t'' + dt'')$ over x'' from x' to x :

$$w_{free}(p_1; x', t'; x, t) = \prod_{x''=x'}^x w_{free}(p_1; x'', t''; x'' + dx'', t'' + dt'') = \prod_{x''=x'}^x [1 - w_{loss}(p_1; x'', t'') dx'']. \quad (15)$$

$w_{loss}(p_1; x'', t'')$ denotes the probability density that a particle with momentum p_1 is destroyed via a collision at (x'', t'') and is expressed by

$$w_{loss}(p_1; x'', t'') dx'' = \int d\Gamma_2 f(p_2; x'', t'') v_{rel} \sigma_{22} dt'', \quad (16)$$

where $v_{rel} = s/(2p_1^0 p_2^0)$ and $dt'' = dx'' (p_1^x/p_1^0)^{-1}$.

We now approximate $w_{loss}(p_1; x'', t'')$ to be the averaged one over p_1 :

$$w_{loss}(p_1; x'', t'') dx'' \approx \int d\Gamma_2 f(p_2; x'', t'') \langle v_{rel} \sigma_{22} \rangle \left\langle \frac{|p_1^x|}{p_1^0} \right\rangle^{-1} dx'' = 2n \langle v_{rel} \sigma_{22} \rangle dx'' = \frac{2dx''}{\lambda_{mfp}}, \quad (17)$$

where λ_{mfp} denotes the particle mean free path. This approximation applies for isotropic cross sections. In general, if the angular distribution is non-isotropic λ_{mfp} has to be replaced by an effective length scale, which is calculated as an average of the differential cross section.

With Eq. (17) we obtain the obvious expression

$$w_{free}(p_1; x', t'; x, t) = \lim_{dx'' \rightarrow 0} \left(1 - \frac{2dx''}{\lambda_{mfp}} \right)^{|x-x'|/dx''} = \exp \left(-\frac{2|x-x'|}{\lambda_{mfp}} \right). \quad (18)$$

Putting Eqs. (12), (14), and (18) into Eq. (10) gives

$$A(x, t) = \int_{-\infty}^{\infty} dx' e^{-\frac{2|x-x'|}{\lambda_{mfp}}} \frac{1}{n} \int d\Gamma'_1 d\Gamma'_2 f(p'_1; x', t') f(p'_2; x', t') v_{rel} \int d\Gamma_1 F_A(p_1) \frac{d\sigma_{22}}{d\Gamma_1}. \quad (19)$$

It is clear that replacing $F_A(p_1)$ by $F_A(p_1) + F_A(p_2)$ will leads to $2A(x, t)$. We now consider particular observables $A(x, t)$ such that F_A is conserved in each collision, i.e., $F_A(p'_1) + F_A(p'_2) = F_A(p_1) + F_A(p_2)$. We then have

$$\begin{aligned}
A(x, t) &= \int_{-\infty}^{\infty} dx' e^{-\frac{2|x-x'|}{\lambda_{mfp}}} \frac{1}{n} \int d\Gamma'_1 d\Gamma'_2 f(p'_1; x', t') f(p'_2; x', t') F_A(p'_1) v_{rel} \int d\Gamma_1 \frac{d\sigma_{22}}{d\Gamma_1} \\
&\approx \int_{-\infty}^{\infty} dx' e^{-\frac{2|x-x'|}{\lambda_{mfp}}} \frac{1}{n} \int d\Gamma'_1 F_A(p'_1) f(p'_1; x', t') \int d\Gamma'_2 f(p'_2; x', t') \langle v_{rel} \sigma_{22} \rangle \\
&= \frac{1}{\lambda_{mfp}} \int_{-\infty}^{\infty} dx' e^{-\frac{2|x-x'|}{\lambda_{mfp}}} A(x', t'). \tag{20}
\end{aligned}$$

The same approximation is made as for w_{loss} in Eq. (17). Equation (20) resembles the one derived in Ref. [22] using "path integral method" in non-relativistic cases.

We emphasize that Eq. (20) holds only if the total F_A is conserved in collisions. For instance, the total particle velocity $\mathbf{p}_1/E_1 + \mathbf{p}_2/E_2$ is not conserved except in case the energy of all particles is same, whereas the total particle momentum rapidity is conserved. Therefore, the rapidity $y(x)$ defined by Eq. (7) obeys Eq. (20), but the hydrodynamic velocity $v_z(x)$ does not. However, the total particle momentum rapidity is not conserved in $2 \rightarrow 3$ or $3 \rightarrow 2$ processes. In this case one has to take detailed balance into account and the sum of the total rapidity of a $2 \rightarrow 3$ and its back reaction is conserved on average. If $y(x)$ is conserved in collisional processes, it obeys Eq. (20).

Equation (20) represents a homogeneous first-order integral equation for $A(x)$. It can easily be shown that the second derivative of $A(x)$ vanishes, which leads to the solution $A(x) = ax + b$, where a and b are constant. We choose the boundary conditions to be $A(x) = -y_{wall}$ for $x < -L/2$ and $A(x) = y_{wall}$ for $x > L/2$ to reproduce the scenario introduced in Sec. I. Since this scenario is symmetric in x we have $b = 0$. To determine a we insert $A(x) = ax$ into Eq. (20) and obtain $a = 2y_{wall}/(L + \lambda_{mfp})$. Finally the rapidity has the following form

$$y(x) = \frac{2y_{wall}}{L + \lambda_{mfp}} x. \tag{21}$$

We recognize the discontinuities of $y(x)$ at the boundaries, which disappear only for vanishing mean free path $\lambda_{mfp} \rightarrow 0$ or long distance $L \rightarrow \infty$. Equation (21) is a new finding and accounts for finite size effects which must be taken into account, if for numerical reasons λ_{mfp}/L cannot be made sufficiently small.

B. Numerical Confirmation

In this subsection we will confirm our finding Eq. (21) by performing numerical transport calculations. We employ the parton cascade BAMPS. Details of numerical operations can be found in Refs. [18, 19]. One important feature of BAMPS is that the model can simulate multiplication and annihilation processes such as the gluon bremsstrahlung process and its back reaction $gg \leftrightarrow ggg$ with full detailed balance. In order to verify the analytic findings we will first employ isotropic cross sections in BAMPS in the following.

The numerical realization of the boundary conditions is as follows. Particles that reach the boundaries $x = \pm L/2$ are removed, which simulates the particle absorption by the plates. Independent of the absorption, the plates emit particles, which pick up the velocities $\pm v_{wall}$ of the plates. Here we treat the plates as thermal reservoirs of particles with the same temperature as those between the plates. The momentum distribution for emitting particles is proportional to the equilibrium Boltzmann distribution $f_{wall}(p)$ and the particle velocity p_x/E :

$$\frac{dN_{em}}{dt d^3p} \sim \frac{p_x}{E} f_{wall}(p) \quad (22)$$

with

$$f_{wall}(p) = g e^{-\frac{p^\mu u_{wall}^\mu}{T}}, \quad (23)$$

where $u_{wall}^\mu = \gamma_{wall}(1, 0, 0, v_{wall})$, $\gamma_{wall} = 1/\sqrt{1 - v_{wall}^2}$, $g = 16$ is the degeneracy factor for gluons in $SU(3)$, and T is the temperature. In the distribution (23) we neglect the quantum statistic factor for bosons and fermions. The rate of emissions can be calculated analytically (see App. A) and is

$$\frac{dN_{em}}{dt} = \frac{1}{4} A_{wall} n_{wall}, \quad (24)$$

where A_{wall} is the transverse area of the plates and n_{wall} is the particle density. In the xy - and xz -plane the boundary conditions are periodic.

Particles between the two plates are initially distributed by the equilibrium form like Eq. (23) with zero velocity. Figure 2 shows the buildup of the rapidity profile. We have chosen $L = 2$ fm, $v_{wall} = 0.5$ ($y_{wall} = 0.55$), and $T = 0.4$ GeV. Only binary collisions with a constant cross section are considered. The mean free path is set to be $\lambda_{mfp} = 0.2$ fm. Collision angles of the binary scatterings are distributed isotropically.

The timescale for the buildup of the rapidity (or velocity) profile can be estimated as the mean diffusion time of particles traveling from one plate to another. For a gaussian diffusion

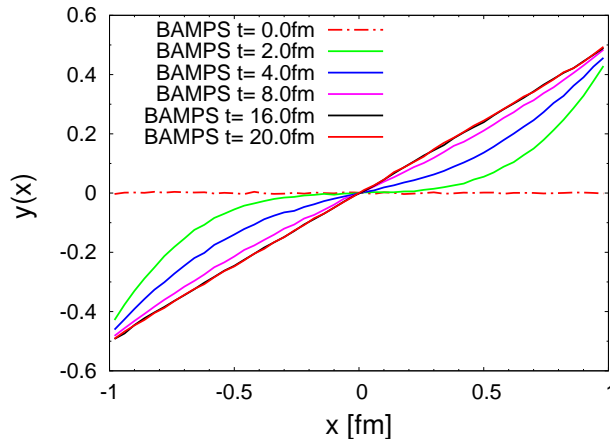


FIG. 2: Build-up with time of the rapidity profile. Results are obtained by averaging 500 events.

process one has [22]

$$\langle x^2 \rangle = 2Dt, \quad (25)$$

where in the non-relativistic limit the diffusion constant D is the ratio of the shear viscosity η to the mass density ρ . For relativistic case we replace ρ by the energy density e . As we will see in the next section, $\eta \approx 1.2654nT\lambda_{mfp} = 0.42e\lambda_{mfp}$ (see Eq. (29)), where $e = 3nT$ is used. Thus,

$$t = \frac{L^2}{2D} = \frac{L^2 e}{2\eta} \approx \frac{L^2}{0.82\lambda_{mfp}}. \quad (26)$$

For our setup we find $t \approx 24$ fm/c, which is consistent with the numerical results shown in Fig. 2.

Figure 3 shows the final rapidity profiles at sufficient long times. Calculations are performed for several mean free paths, in order to demonstrate the finite size effect. The differential cross sections are momentum-independent, i.e. isotropic. The lines present the analytical results given via Eq. (21), while the symbols show the numerical values. One can see an excellent agreement, although approximations are made to obtain Eq. (21). This indicates the validity of the approximations for using isotropic cross sections.

On the contrary, when using the pQCD cross sections for gluons, which strongly depend on the invariant mass s one will have deviations from Eq. (21). The elastic and gluon bremsstrahlung process and its back reaction implemented in BAMPS are based on pQCD matrix elements given in Ref. [18]. Although the numerically extracted rapidity profile is different from the analytical form Eq. (21), it is still linear in x . Replacing λ_{mfp} in Eq. (21) with an effective scale λ_{eff} one obtains the general formula. Using pQCD cross sections λ_{eff}

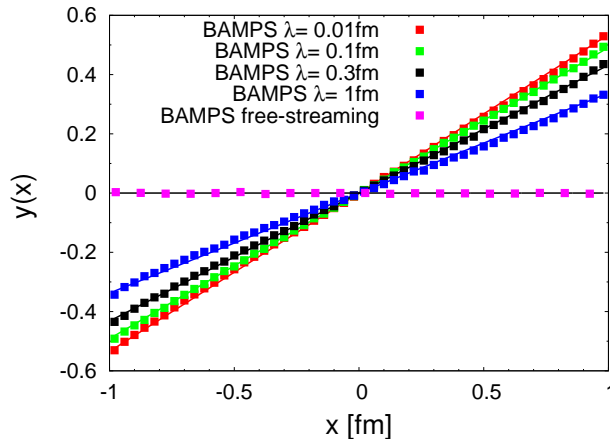


FIG. 3: Rapidity profiles for different mean free paths, $\lambda_{mfp} = 0.02, 0.2, 2, \infty$ fm. Constant cross sections and isotropic distribution of the collision angle are considered. The numerical results from BAMPS (symbols) are compared with the analytical ones (lines) given by Eq. (21).

has to be extracted numerically. Qualitatively, λ_{eff} for pQCD interactions should be larger than λ_{mfp} , since pQCD-based processes prefer small angle scatterings and thus, are not as efficient for momentum transport as scatterings with isotropic angular distribution.

IV. EXTRACTION OF SHEAR VISCOSITY

In stationary states we can use the Navier-Stockes's formula Eq. (2) to calculate the shear viscosity η . For the particular setup shown in Fig. 1, Eq. (2) is simplified to

$$\pi^{xz} = -\eta \frac{d\gamma v_z(x)}{dx} \quad (27)$$

with $\gamma = 1/\sqrt{1 - v_z^2(x)}$. Using Eq. (21) for $v_z(x) = \tanh y(x)$ we obtain

$$\eta = -\pi^{xz} \sqrt{1 - v_z^2(x)} \frac{L + \lambda_{eff}}{2y_{wall}}. \quad (28)$$

(Here λ_{mfp} replaced by λ_{eff} .) π^{xz} and $v_z(x)$ are extracted from BAMPS (the results of $v_z(x)$ are already shown in the previous section), whereas λ_{eff} is obtained by fitting $y(x)$.

Results for isotropic constant cross sections are presented in Sec. IV A. Section IV B contains results for full pQCD interactions.

A. Elastic isotropic constant cross sections

Elastic isotropic constant cross sections are meant that cross sections for elastic binary collisions are constant and the distribution of collision angle is isotropic. In this case the shear viscosity of an ultrarelativistic Maxwell-Boltzmann gas is well known [24]:

$$\eta^{NS} \approx 1.2654 \frac{T}{\sigma} = 1.2654 nT \lambda_{\text{mfp}}. \quad (29)$$

Equation (29) serves as a benchmark to check the numerical methods applied to calculate shear viscosity.

Setups for numerical calculations are $L = 2$ fm, $v_{\text{wall}} = 0.5$, and $T = 0.4$ GeV. Results are averaged over $N_{\text{events}} = 2000$ events. Figure 4 shows the numerically extracted shear viscosity from Eq. (28) in each bin of size $\Delta x = 0.2$ fm. The mean value is in good agreement

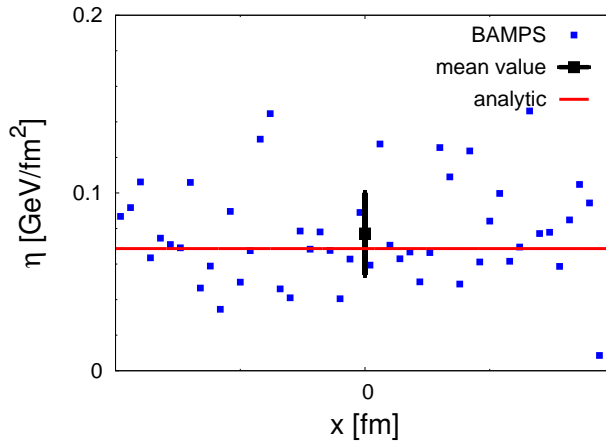


FIG. 4: Shear viscosity extracted from BAMPS and compared to the analytical result from Eq. (29) for $\lambda_{\text{mfp}} = 0.02$ fm.

with the analytical one from Eq. (29) within the standard deviation, which decreases with $1/\sqrt{N_{\text{events}}}$.

Of course this method for the extraction of shear viscosity can only be applied, when the particle system has relaxed to a stationary state. The relaxation time can be estimated according to Eq. (26). The relaxation time is inversely proportional to the mean free path and thus the extraction of shear viscosity for nearly perfect fluids with high N_{events} is time-consuming.

In Fig. 5 we show the mean shear viscosity with the standard deviation as a function of mean free path. The agreement with the analytical results (line) is perfect. This confirms the

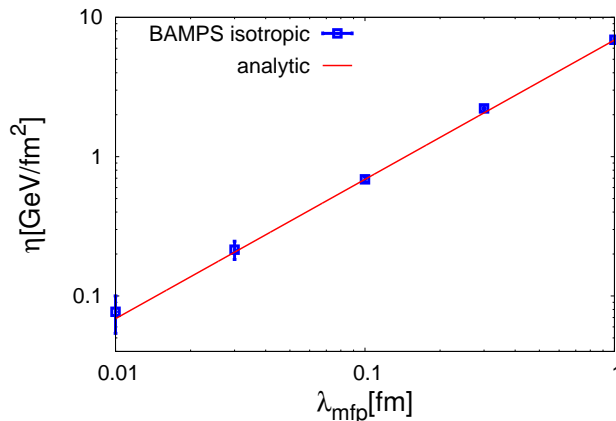


FIG. 5: Shear viscosity as a function of mean free path.

proposed method for extracting the shear viscosity for relativistic systems from numerical calculations.

B. pQCD interactions

In this subsection the results on the shear viscosity are presented for a system of gluons. For gluon interactions elastic $gg \rightarrow gg$ and inelastic $gg \leftrightarrow ggg$ in leading-order pQCD based processes are included. For a more detailed discussion refer to Ref. [18].

Setups for this case are $L = 40$ fm, $v_{\text{wall}} = 0.5$, and $T = 0.4$ GeV. L has to be chosen appropriately as the mean free path increases with decreasing coupling constant α_s . Running coupling is not implemented in the presented BAMPS calculations.

The extracted mean values of the shear viscosity to entropy ratio η/s are given in Table I and also shown in Fig. 7 with the resulting standard deviations of the simulations. The entropy density is taken by its equilibrium value $s = 4n$.

TABLE I: η/s at various α_s .

α_s	0.01	0.03	0.1	0.2	0.3	0.5	0.6
$\eta/s_{2 \rightarrow 2}$	192.5 ± 23	32.6 ± 3.49	5.76 ± 0.63	2.25 ± 0.2	1.35 ± 0.14	0.64 ± 0.064	0.55 ± 0.06
$\eta/s_{2 \rightarrow 2, 2 \leftrightarrow 3}$	43.6 ± 5.2	8.22 ± 0.66	0.87 ± 0.09	0.26 ± 0.03	0.17 ± 0.01	0.1 ± 0.01	0.08 ± 0.01

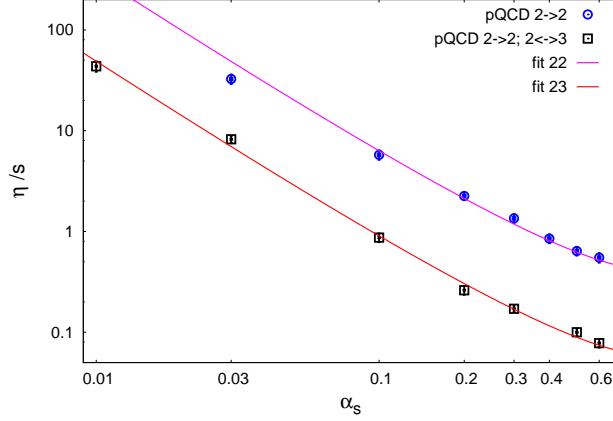


FIG. 6: Shear viscosity to entropy density ratio at various α_s .

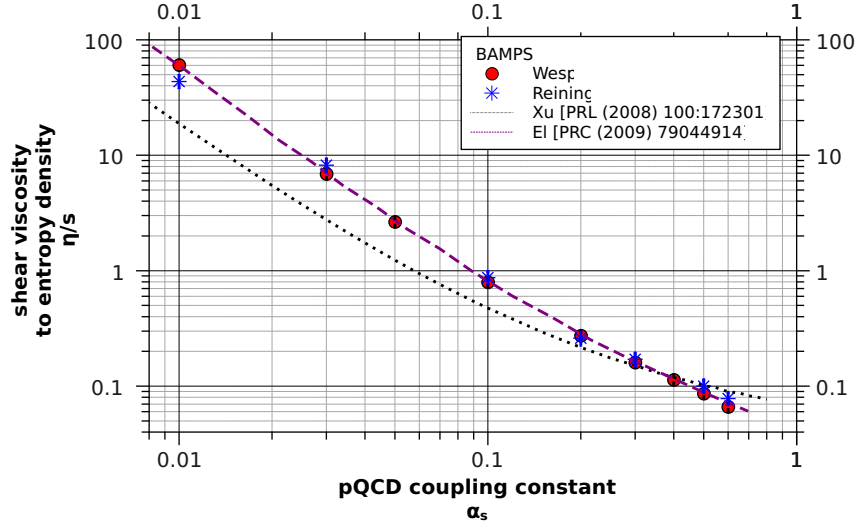


FIG. 7: Shear viscosity to entropy density ratio at various α_s . Comparisons with other calculations using the same matrix elements for gluon interactions are made (more in text).

The new results are compared to values by Xu et al. [20], El et al. [21] and Wesp et al. [26]. Xu et al. identified the shear viscosity coefficient from the Navier-Stokes equation and used a gradient expansion in the Boltzmann equation. Calculating the second moment of the Boltzmann equation they obtained the shear viscosity coefficient in terms of the transport collision rate defined in Ref. [20]. El et al. derive the shear viscosity coefficient from the entropy principle, which also can be applied to derive the Israel-Stewart equations. For their derivation El et al. used Grad's approximation for the off-equilibrium distribution

function and obtained an expression for the shear viscosity similar to the one introduced by Xu et al., but with a slightly different definition of transport collision rate. The results from Wesp et al. [26] originate from equilibrium fluctuations. Here the Green-Kubo relations are employed to extract the shear viscosity. We see a good agreement with all three calculations for $\alpha_s > 0.2$. For $\alpha_s < 0.2$ our data is in excellent agreement with the data from El et al. as well as Wesp et al. We observe the $1/(\alpha_s^2 \log(1/\alpha_s))$ scaling behavior expected from Ref. [16, 27].

Applicability of the methods by Xu et al. and El et al. crucially depends on the chosen parametrisations for the off-equilibrium distribution functions. In particular the momentum dependence of the off-equilibrium correction to the equilibrium distribution was chosen differently by these authors, which might explain the deviations between their results (Compare also the discussion in Ref. [26].)

V. CONCLUSIONS AND OUTLOOK

In this work we started with the classical picture of shear viscosity and shear flow. We demonstrated that the classical picture of a linear velocity field does not apply to relativistic systems. Rather, we found that velocity fields have a non-linear form, whereas the rapidity increases in fact linearly.

We also derived an analytical expression for the rapidity and velocity profiles in systems where the mean-free path is non-zero. With an increasing mean-free path to system size ratio the slope of the rapidity profile decreases and finite size effects are not negligible anymore.

We employed the numerical transport model BAMPS to create the velocity and rapidity profiles, compared the numerical results to our theoretical findings and observed an almost perfect agreement. The stationary gradient allows us to apply the relativistic Navier-Stokes equation to calculate the shear viscosity coefficient η . We found again a perfect agreement to the analytical value derived from kinetic theory [24]. The method proposed here to calculate the shear viscosity coefficient is thus perfectly suitable for other microscopic transport descriptions.

Furthermore we have then used this setup to calculate the shear viscosity to entropy density ratio in a numerical simulation with elastic and inelastic pQCD processes implemented in BAMPS for fixed coupling constant α_s , which is varied from $= 0.01$ to 0.6 . We compared

our results with previously published results [20, 21] and also with a very recent work based on the Kubo relation [26] and found a very good agreement.

Acknowledgements

The authors are grateful to the Center for the Scientific Computing (CSC) at Frankfurt for the computing resources. FR, CW and IB are grateful to ‘‘Helmholtz Graduate School for Heavy Ion research’’. AE and FR acknowledge support by BMBF. This work was supported by the Helmholtz International Center for FAIR within the framework of the LOEWE program launched by the State of Hesse.

Appendix A

We calculate the number of particles ΔN with a thermal Maxwell-Boltzmann distribution, passing through a wall of area A . The number of particles passing through a wall orthogonal to the x -direction in a small timestep Δt is equal to the number of all particles with distance $\Delta x < -v_x \Delta t$ from the wall:

$$\Delta N = \int_{v_x < 0} \frac{d^3 p}{(2\pi)^3} \int_A dy dz \int_{0 < x < -v_x \Delta t} dx f(\mathbf{p}) = - \int_{v_x < 0} \frac{d^3 p}{(2\pi)^3} A v_x \Delta t f(\mathbf{p}) \quad (\text{A1})$$

$$\begin{aligned} \frac{\Delta N}{\Delta t} &= - \int_{v_x < 0} \frac{d^3 p}{(2\pi)^3} A v_x f(\mathbf{p}) \\ &= -A \int_{v_x < 0} \frac{d^3 p}{(2\pi)^3 E} p_x f(\mathbf{p}) = -A \int_{v_x < 0} \frac{d^3 p}{(2\pi)^3 E} p_x g e^{-\frac{u^\mu p_\mu}{T}} \\ &= -\frac{gA}{(2\pi)^3} \int_\pi^{2\pi} d\phi \int_0^\infty p_t dp_t \int_{-\infty}^\infty dy p_t \cos(\phi) e^{-\frac{p_t \cosh(y+\beta)}{T}} \end{aligned} \quad (\text{A2})$$

where $u^\mu = (\cosh(\beta), 0, 0, \sinh(\beta))$. After the transformation of variables $y \rightarrow y - \beta$ the dependence on the boost velocity drops out:

$$\begin{aligned} \frac{\Delta N}{\Delta t} &= -\frac{gA}{(2\pi)^3} \int_\pi^{2\pi} d\phi \int_0^\infty p_t dp_t \int_{-\infty}^\infty dy p_t \cos(\phi) e^{-\frac{p_t \cosh(y)}{T}} \\ &= \frac{2gA}{(2\pi)^3} \int_0^\infty dp_t \int_{-\infty}^\infty dy p_t^2 e^{-\frac{p_t \cosh(y)}{T}} \end{aligned}$$

$$= \frac{2gA}{(2\pi)^3} \int_{-\infty}^{\infty} dy \frac{2T^3}{\cosh^3(y)} = \frac{gAT^3}{(2\pi)^2} = \frac{nA}{4}$$

where $n = gT^3/\pi^2$ is the density in the local rest frame.

-
- [1] K. H. Ackermann et al. [STAR Collaboration], Phys. Rev. Lett. **86** (2001) 402;
- [2] S. S. Adler et al. [PHENIX Collaboration], Phys. Rev. Lett. **91** (2003) 182301;
- [3] B. B. Back et al. [PHOBOS Collaboration], Phys. Rev. Lett. **89** (2002) 222301;
- [4] K. Aamodt *et al.* [The ALICE Collaboration], [arXiv:1011.3914 [nucl-ex]]
- [5] H. Song, U.W. Heinz, Phys. Rev. C **77** (2008) 064901.
- [6] M. Luzum, P. Romatschke, Phys. Rev. **C78**, 034915 (2008). [arXiv:0804.4015 [nucl-th]].
- [7] U. W. Heinz, arXiv:0901.4355 [nucl-th].
- [8] D. A. Teaney, arXiv:0905.2433 [nucl-th].
- [9] H. Niemi, G. S. Denicol, P. Huovinen, E. Molnar, D. H. Rischke, [arXiv:1101.2442 [nucl-th]].
- [10] B. Schenke, S. Jeon, C. Gale, [arXiv:1102.0575 [hep-ph]].
- [11] H. Song, S. A. Bass, U. W. Heinz, [arXiv:1103.2380 [nucl-th]].
- [12] Z. Xu, C. Greiner, H. Stoecker, Phys. Rev. Lett. **101**, 082302 (2008).
- [13] G. Ferini, M. Colonna, M. Di Toro, V. Greco, Phys. Lett. **B670**, 325-329 (2009).
- [14] P. Kovtun, D. T. Son and A. O. Starinets, Phys. Rev. Lett. **94**, 111601 (2005)
- [15] P. F. Kolb, P. Huovinen, U. W. Heinz, H. Heiselberg, Phys. Lett. **B500**, 232-240 (2001).
- [16] P. Arnold, G. D. Moore, L. G. Yaffe, J. High Energy Phys. **0305** (2003) 051.
- [17] M. Bluhm, B. Kampfer, K. Redlich, [arXiv:1011.5634 [hep-ph]].
- [18] Z. Xu and C. Greiner, Phys. Rev. C **71** (2005) 064901
- [19] Z. Xu and C. Greiner, Phys. Rev. C **76** (2007) 024911
- [20] Z. Xu and C. Greiner, Phys. Rev. Lett. **100**, 172301 (2008)
- [21] A. El, A. Muronga, Z. Xu and C. Greiner, Phys. Rev. C **79**, 044914 (2009)
- [22] F. Reif *Fundamentals of Statistical and Thermal Physics*, Waveland Pr Inc (2008)
- [23] F. Reining, *Untersuchung von Scherfluss und -Viskosität in einer partonischen Kaskade* - unpublished, Diploma thesis, Goethe Universität Frankfurt 2009,
- [24] S. R. de Groot, W. A. van Leeuwen, Ch. G. van Weert, *Relativistic Kinetic Theory: Principles*

and Applications North Holland (1980)

- [25] L. D. Landau and E. M. Lifshitz, *Fluid Dynamics*, Second Edition, Butterworth-Heinemann (1987).
- [26] C. Wesp et al., *Calculation of shear viscosity using Green-Kubo relations within a parton cascade*, paper in preparation
- [27] G. Baym, H. Monien, C. J. Pethick and D. G. Ravenhall, *Phys. Rev. Lett.* **64** (1990) 1867.